Opto-Electronics Plus

High bonding strength metal film on ceramic fabricated by the catalysis of exsolved nanoparticles combining DLP-based ceramic 3D printing

Kun Zhang, Shuo Liu, Lehan Wang, Huaixiang Zan, Yushi Chu and Jianzhong Zhang

Citation: Zhang K, Liu S, Wang LH, et al. High bonding strength metal film on ceramic fabricated by the catalysis of exsolved nanoparticles combining DLP-based ceramic 3D printing. *Opto-Electronics Plus* **2**, 260008(2026).

Received: 13 April 2026; Accepted: 19 May 2026; Published online: 22 June 2026

Opto-Electronics Plus

Article

June 2026, Vol. 2, No. 2

Open Access

High bonding strength metal film on ceramic fabricated by the catalysis of exsolved nanoparticles combining DLP-based ceramic 3D printing

Kun Zhang[1], Shuo Liu[1], Lehan Wang[2], Huaixiang Zan[2], Yushi Chu[1,2]* and Jianzhong Zhang[1]*

Abstract: Here, we report that metal films with high bonding strength are deposited on alumina ceramic substrates by virtue of alumina light curing technology, the interface of which can withstand repeated thermal shocks from 1073 K to 77 K. Unlike conventional nickel particles deposited on alumina, exsolved Ni particles are epitaxially bonded to the substrate and catalyze the formation of metal films via chemical deposition, generating the "nanopinning effect". Furthermore, we reveal the exsolution mechanism of particle and weakened Ostwald ripening effect critical for future design of exsolution-based reducible ceramic materials for chemical catalysis and other functionalities. In addition, the metallized ceramic heater and circuit board are fabricated, which show excellent thermal resistance and conductivity respectively. The proposed technique free from traditional sensitization and activation processes opens up a promising strategy of implementing complicated three-dimension constructions with high bonding strength metal films.

Keywords: DLP-based ceramic 3D printing; metal film; high bonding strength; interface; ceramic electronics

DOI:

Citation: Zhang K, Liu S, Wang LH et al. High bonding strength metal film on ceramic fabricated by the catalysis of exsolved nanoparticles combining DLP-based ceramic 3D printing. *Opto-Electron Plus* **2**, 260008 (2026).

1 Introduction

Metallized ceramics have been extensively utilized in electronics due to their excellent physical, chemical and mechanical properties[1–2]. Electroless plating (EP) is a priority technique achieving metal films for dielectric substrates whose surfaces are unable to activate autocatalytic reactions, and the vast majority of catalytic particles are prepared by deposition methods before plating, which are although widely applicable, provide cumbersome and susceptible pretreatment process[3–5]. This generally leads to limited role of metal particles except for catalyzing. Besides, coarsening, intermediates or post heat treatment are typical processes for chemical deposition to enhance the bonding strength of metal films by forming the mechanical interlocking or primary bonds. While these solutions suffice for most scenarios, their complexity can render them ineffective and even detrimental to substrates or films[3,6–8].

As a vital technique, ceramic light curing provides the possibilities for the direct and fast production of ceramic parts with extremely specific microstructure and complex geometries. Thereinto, it allows for a convenient metal ion doping in superficial layer before the sintering process. Actually, approach of the exsolution from solid oxide lattices to form well-dispersed metal particles with superior stability and longevity has become attractive, the process of which involves the migration of metal ions from substrate to the surface under reducing conditions[9–11]. Studies have demonstrated that catalytically active transition metals can be substituted on the B-site of perovskite or react with alumina to generate spinel, and exsolved on the surface as metal particles following reduction, with applications in catalysis ranging from methane reforming to solid oxide electrolysis cells, etc[12–15]. Nevertheless, metal-support interaction (MSI) may occur in the process of high-temperature exsolution,

Received: 13 April 2026

Accepted: 19 May 2026

Published online: 22 June 2026

[1]Key Laboratory of In-fiber Integrated Optics of Ministry of Education, College of Physics and Optoelectronic Engineering, Harbin Engineering University, Harbin 150001, China; [2]Fiber Optical Sensing Center for Excellence, Yantai Research Institute, Harbin Engineering University, Yantai 264000, China.

*Correspondence: YS Chu, E-mail: chuyushi@hrbeu.edu.cn; JZ Zhang, E-mail: zhangjianzhong@hrbeu.edu.cn

which will affect the particle morphology, chemical composition and suboxide encapsulation behavior, thus having considerable impacts on the activity, selectivity and stability of supported metal catalysts[16–18]. But the effects on the application of EP are unclear.

Here we reveal that nickel particles exsolved from the co-sintered alumina ceramic under reduction atmosphere are epitaxially bonded to the surface parent nickel aluminate spinel phase, maintaining their stability and catalytic characteristic for EP. We also provide critical insights into the exsolution and stability of particle, and the effect of MSI on EP. Furthermore, the particles distributing on the surface of alumina ceramic uniformly are found to have a new functionality namely "nanopinning", thereby generating a stronger metal-oxide interface between metal film and substrate. Then, alumina ceramic-based copper wire circuit board and nickel-phosphorus alloy wire heater circuit are fabricated respectively, showing excellent conductivity and thermal resistance. The proposed technique offers an integrated strategy of implementing complicated metallized three-dimension constructions, and thus achieves high bonding strength of metal films efficiently compared to traditional sensitization and activation processes.

2 Results

2.1 Fabrication strategy, structure and morphological characterization

In this work, we employ exsolved metal particles to achieve high bonding strength between metal film and substrate, which can be ascribed to the nanopinning effect, similar to the phenomenon of shell's byssus attaching to stone (Fig. 1(a)). Metallized alumina structures were fabricated integrating unconfined 3D printing process with versatile chemical deposition, simplifying the pre-treatment procedures of degreasing, etching, sensitizing and activating before plating (Fig. S1 in the Supplementary Information).

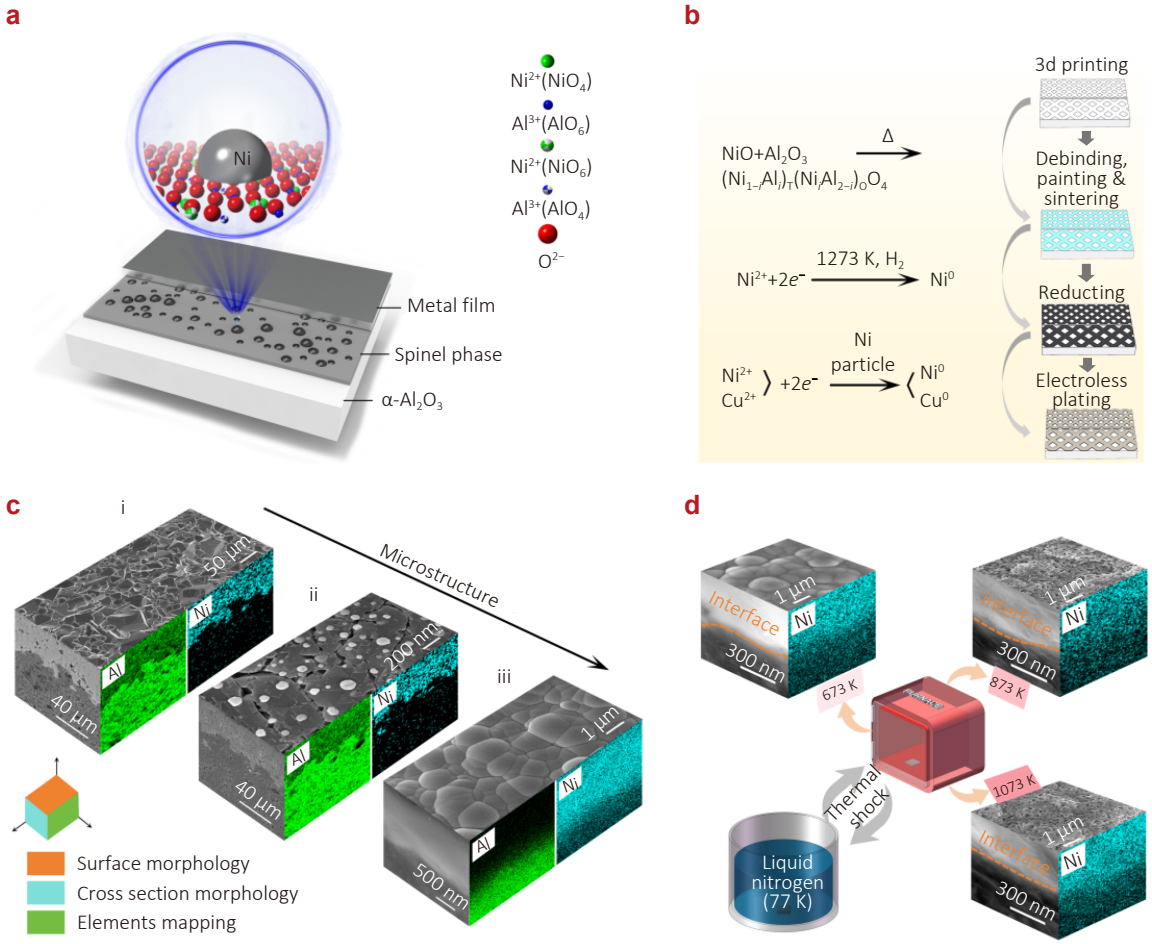

Fig. S1 | Fabrication of metallized alumina ceramic. (a) A schematic diagram of metal film on alumina ceramic. NiO_4 and NiO_6 represent Ni^{2+} in tetrahedral and octahedral sites respectively, the same as AlO_4 and AlO_6. (b) Primary chemical reactions in each process of the fabrication of metal films on alumina. (c) Morphology and cross-sectional EDS elemental mapping of samples after co-sintering (i), reducing (ii) and Ni-P alloy EP (iii). (d) Top surface morphology and interface between metal films and substrate after different thermal shock tests.

The main reactions in each process are shown in Fig. 1(b). Thereinto, $NiAl_2O_4$, also denoted as $(Ni_{1-i}Al_i)_T(Ni_iAl_{2-i})_OO_4$, is largely a inverse spinel with the reported inversion parameter i over 0.8 at room temperature[19].

Coarse surface and dense structure (Fig. 1(c-i), Fig. S2(a) and S2(b) in the Supplementary Information) were generated after co-sintering at the temperature of 1600 °C. During the process, nickel oxide (NiO) nanoparticles reacted with alumina substrate completely to form the new nickel aluminate phase, as confirmed by the energy-dispersive spectroscopy (EDS) elemental mapping (Fig. 1(c-i), Fig. S2(d) in the Supplementary Information) and X-ray diffraction results (Fig. S2(f) in the Supplementary Information). Nickel aluminate spinel can be reduced in a reducing atmosphere[20], which is also thermodynamically favourable at 1273 K due to the negative value of Δ_rG for the $NiAl_2O_4$ reduction (Eq. (1), Supplementary Text).

$$NiAl_2O_4(s) \overset{1273K,H_2}{\longleftrightarrow} Ni(s) + Al_2O_3(s) + H_2O(g),$$
$$\Delta G_r \approx -616\ \mathrm{kJ/mol}, \tag{1}$$

As shown in Fig. 1(c-ii), small spherical nanoparticles are observed on the surface after reducing treatment, most of which are less than 300 nm (Statistics in Fig. S2(c) in the Supplementary Information). EDS and X-ray diffraction patterns depicted in Fig. S2(e) and S2(g) in the Supplementary Information certified the metallic nickel nanoparticles, as well as the reserved spinel phase which is associated with the insufficient reduction or incomplete phase transformation[21]. In addition, the exsolution of Ni results in cracks on surface, which can be ascribed to the diffusion of vacancies toward the surface[19]. The reconstructed surface, with enhanced surface area and rough surface structuring at length scales from nanometers to microns, is expected to have a positive influence on the bonding strength between plated metal films and substrate. The exsolved Ni particles catalyze the deposition of Ni ions to form Ni-P alloy film during EP, depicted in Fig. 1(c-iii). In particular, it should be noted that samples to be co-sintered made by dipping method are not able to exsolve Ni particles from surface when the sintering temperature exceeds 1550 °C, indicating a requirement on the concentration of NiO suspension due to the migration of Ni ions in alumina. Figure S3 in the Supplementary Information showed the similar results compared to screen-printing method using lower concentration of NiO dispersion except for the different distribution of particle sizes.

Three different temperature intervals of repeated thermal shocks were taken to examine the plated Ni-P alloy film and results demonstrated that the strong interface bonding can bear the shock of approximately 1000 K (Interfaces shown in Fig. 1(d)), although a slight oxidization on surface was observed at the elevated temperatures of 873 K and 1073 K.

2.2 Interface of particle–substrate

As shown in Fig. 2(a), the STEM-EDS micrograph and elemental mapping also confirmed that Ni nanoparticle was exsolved from substrate. High-resolution TEM (HRTEM) imaging (Fig. 2(b)) of the particles exsolved on $(\bar{1}\bar{1}1)$ terminations of nickel aluminate spinel revealed their epitaxic relationship, which was highlighted by the depiction of nickel aluminate spinel $(1\bar{1}1)$ planes aligned to the $(1\bar{1}1)$ planes of the Ni lattice. Figure 2(e) depicted the selected area electron diffraction (SAED) patterns containing diffractions from the matrix and a nickel particle. The patterns correspond to the [011], $[\bar{1}12]$ and [114] zone axes of surface layer $NiAl_2O_4$, while nickel diffractions corresponding to the same zone axis are also visible respectively in each case, indicating that particles are metallic single crystal in nature and epitaxial with respect to the parent spinel. A more detailed analyses of the proposed orientation relationship are given in Fig. 3(c) and Fig. S4 in the Supplementary Information. It should be noted that dislocations are likely to occur in the metal lattice to accommodate the lattice mismatch.

From the concentration profile obtained using atomic-resolution TEM-EDS line scanning, it is observed that there is a gradual change from the Ni particle to the matrix. Notably, substrate near the boundary remains spinel structure consistent with the XRD results (Supplementary Fig. 2(g)) though the concentration of Ni approaches zero. This observation can be explained by the fact that the transformation of spinel lattice does not yet finish under the reducing condition, thus generating metastable structure[21]. Moreover, the deficiency of oxygens (or oxygen vacancies) are also confirmed in the structure.

In addition, the phenomenon of Ni particles socketed into the matrix is also observed (Fig. S5 in the Supplementary Information), which is similar to the situation of Ni particles exsolved from perovskite[22]. Overall, the fact the metal lattice is growing from the oxide lattice might significantly increase adhesion between metal and oxide phases, thus facilitating the formation of "nanopinning" when plating metal films.

2.3 Atomic scale insights into the behaviors of particle exsolving and metal film bonding

It is important to address the question how the exsolution phenomenon occurs in $NiAl_2O_4$ phase. A reasonable assumption is proposed that spontaneous exsolution behavior takes place in $NiAl_2O_4$ when amounts of oxygen vacancies and Ni vacancies could be introduced instantaneously by reducing, and the NiO can be converted to the Ni exsolution subsequently (Fig. 3(a) and 3(b)). The mechanism of exsolution can be qualitatively expressed as point defect (Schottky-type defect) reactions by using the Kröger-Vink notation as follows:

$$Ni_M^{\times} + O_O^{\times} \leftrightarrow NiO + V_O^{\cdot\cdot} + V_{Ni}^{''}, \tag{2}$$

$$NiO \leftrightarrow Ni_{exsolution} + \frac{1}{2}O_2, \tag{3}$$

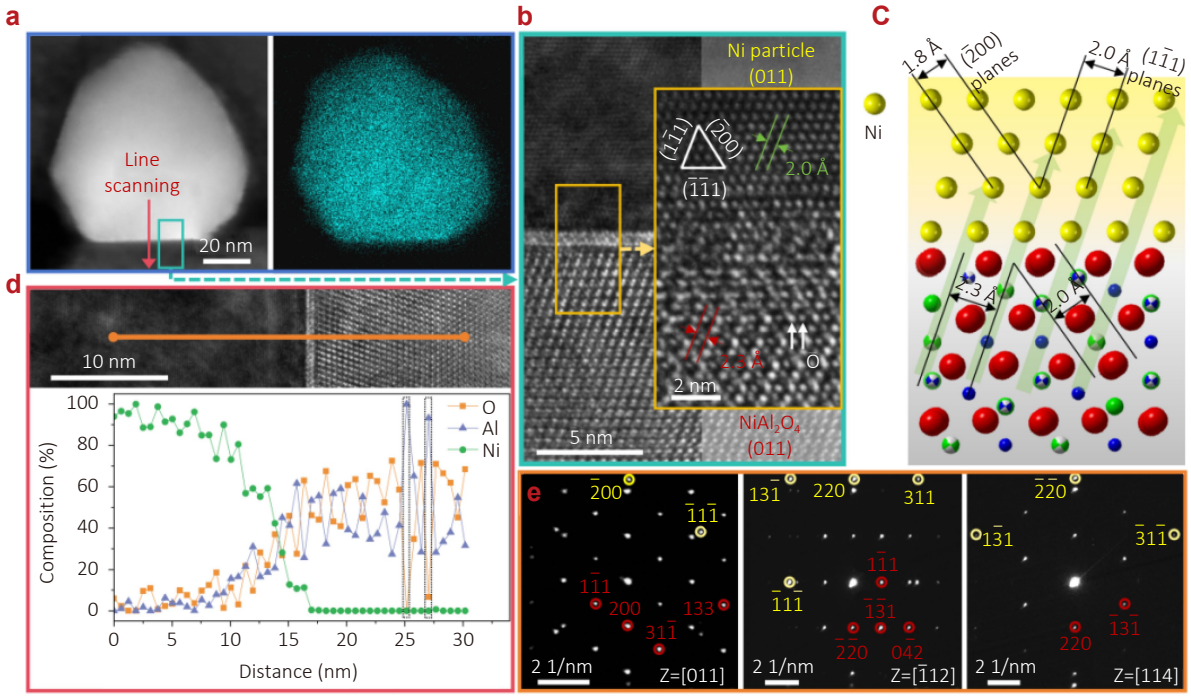

Fig. S2 | Interface of the exsolved particle and substrate. (a) HAADF-STEM image of exsolved particle with the EDS elemental map of Ni. (b) HRTEM micrograph detail of the interface between Ni particle and surface metastable nickel aluminate spinel highlighting the corresponding atomic planes and orientations. (c) Schematic atomic model of the metal–spinel orientation relationship based on b. (d) TEM-EDS line scanning showing the compositional profile across the interface of the Ni particle and matrix. (e) Orientation relationship between exsolved particle and parent $NiAl_2O_4$ for the sample in a.

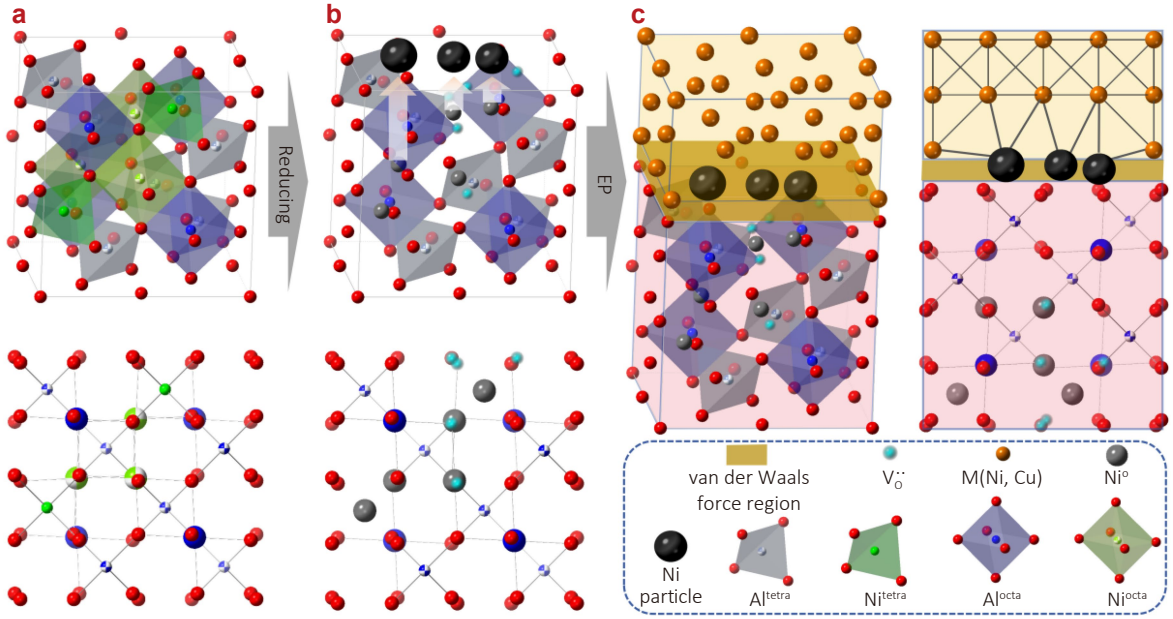

Fig. S3 | Exsolution of Ni from nickel aluminate spinel and catalysis for EP. Schematic of lattice structures of the formed disordered spinel $NiAl_2O_4$ phase after sintering (a) and reducing (b) as well as the combination between metal film and matrix after EP (c). C illustrates the exsolved Ni particles connect with metal film in the form of metallic bond, and metal film adheres to the substrate by weak electrostatic attraction (van der Waals force) except the occupied sites by Ni particles on surface.

where $Ni_M^{\times}$ denotes Ni ion in the tetrahedral or octahedral sites with the net charge zero, $O_O^{\times}$ denotes oxygen in the oxygen site with the net charge zero, $V_O^{\cdot\cdot}$ denotes the oxygen ion vacancy with the net charge +2, V_{Ni}'' denotes the Ni ion vacancy with the net charge −2.

Calculations indicate that metal ion segregates more easily at the presence of oxygen vacancy in CeO_2 and perovskite[9,23–24]. Hence, it is rational to speculate that the Ni

co-segregates with the nearby oxygen vacancy towards the surface. Notably, particles tended to exsolve continuously instead of aggregating under longer reduction time (Fig. S6(a) and S6(b)) in the Supplementary Information, which could be ascribed to the weakened Ostwald ripening effect resulted from the high adhesion energy between metal and substrate[25–27]. Nonetheless, the migration of Ni towards the inside were limited even under relatively long reduction time at high temperature (Fig. S6(c), S6(d) and S6(e) in the Supplementary Information).

In consideration of the high reduction temperature, MSIs such as suboxide encapsulation may simultaneously occur during the exsolution process, though Al_2O_3 (or metastable $NiAl_2O_4$ here) is often considered as weak MSI support[15]. However, the quick starting of the subsequent EP appeared to show that little impact was made on the chemical catalysis effect of the potentially enclosured Ni particles. Specifically, pull-off tests to estimate the metal film adhesion (Fig. S7 in the Supplementary Information) indicated that a strong interface was generated for all reduction conditions. Figure 3(c) showed the situation that metal film connects with alumina substrate. The behavior that Ni nanoparticles are epitaxially bonded to the substrate is equivalent to the formation of micro-area interdiffusion between metal film and substrate, which is called "nanopinning effect" here. Additionally, Ni particles embedding in substrate provides additional mechanical anchoring effect. Hence, the mechanism of strong adhesion of metal film can be attributed to the integration of interdiffusion theory and mechanical interlocking (aroused by rough surface and embedded Ni particles).

2.4 Fabrication of metallized ceramic structures

In order to demonstrate a typical application utilizing the high thermal stability of the metallized Al_2O_3 ceramic, the Ni-P alloy plated grid conductors with different line widths were applied to a ceramic heater. A DC voltage was supplied to the thin-film heater through silver contacts at the two ends (Fig. 4(a-i)) and the temperature distribution of the heater was recorded using an infrared (IR) thermal imager . A uniform temperature distribution was observed due to the excellent thermal and electrical conductivity of the plated Ni conductors, as well as relatively high surface quality of the Ni heater (Fig. 4(a-ii), Fig. S8(a) in the Supplementary Information). Furthermore, the high-temperature oxidation resistance of the Ni-P alloy film was evaluated by heating the sample in air. For temperature rise tests, samples are maintained for 1 h at each elevated temperatures and cooling down to room temperature for measuring. The recorded electrical resistance of the Ni-P alloy film on ceramic substrate indicated that the produced metallized ceramic can endure up to at least 400 °C for long-term operation (Fig. 4(b-i) and 4(b-ii)). The post-experimental surface morphologies and element analysis, cross-sectional interface, and phase transformation reconfirmed its high-temperature resistance property (Fig. S9 in the Supplementary Information). In addition, the variation of electrical resistance after thermal shock tests further specified the applicable condition that the nearly open-circuit state resulted from film cracking should be avoided, though the interface bonding was strong enough to withstand the thermal shocks (Fig. 4(b-iii)).

Ceramic circuit boards have been extensively utilized in aerospace, power generation and 5G communications due to their high thermal conductivity and heat resistance, excellent dielectric properties, and mechanical strength[28–29]. In this work, the combination of digital light processing (DLP) 3D printing technique and copper film EP enables the creation of circuits without the need for etching. The designed and manufactured copper-plated circuit board soldered with corresponding components has been verified to achieve the expected function totally (Fig. 4(c) and supplementary movie). To confirm the mechanical property of printed substrate and surface condition after EP, bending strength sintered at 1550 °C and 1600 °C and surface roughness under different plating time were measured. Results indicate that the bending strength all exceed 300 MPa and the surface roughness can be decreased to 8 μm by increasing plating time to 9h (Fig. S8(b) to S8(e) in the Supplementary Information). As a demonstration of the freeforming of high adhesive metal films on ceramic, the selectively metallized industrial applied power battery connector, mountains in Mars and dragon were fabricated using the method in this work (Fig. 4(d-f)).

3 Discussion

In this work, we reveal the unique interface developing between the exsolved Ni particles and parent substrate that leads to a emergent nanopinning effect of great utility for EP. Thus, it provides an attractive route for the freeforming of high adhesive metal films on ceramic in combination of 3d printing technique, beyond the capabilities of conventional deposition methods. In particular, the integrated co-sintering for catalytic element and the exsolution process may enable the production of epitaxial bonded or even socketed metal particles through a single-step reduction treatment. In addition, the epitaxial orientation relationship between particle and substrate decrease the overall stress. We also provide the critical insights into the mechanism of particle exsolution, which is crucial for reducible ceramic materials such as some spinels or olivines. For the applications, the proposed method of preparing nickel-phosphorus alloy wire heater circuit that exhibits excellent conductivity and thermal shock resistance has great potential in the industry of ceramic heaters with three-dimension structures. Furthermore, Compared with monolayer Direct Plating Copper (DPC), Direct Bonded Copper (DBC) and Active Metal Brazing (AMB), the approach to fabricating alumina

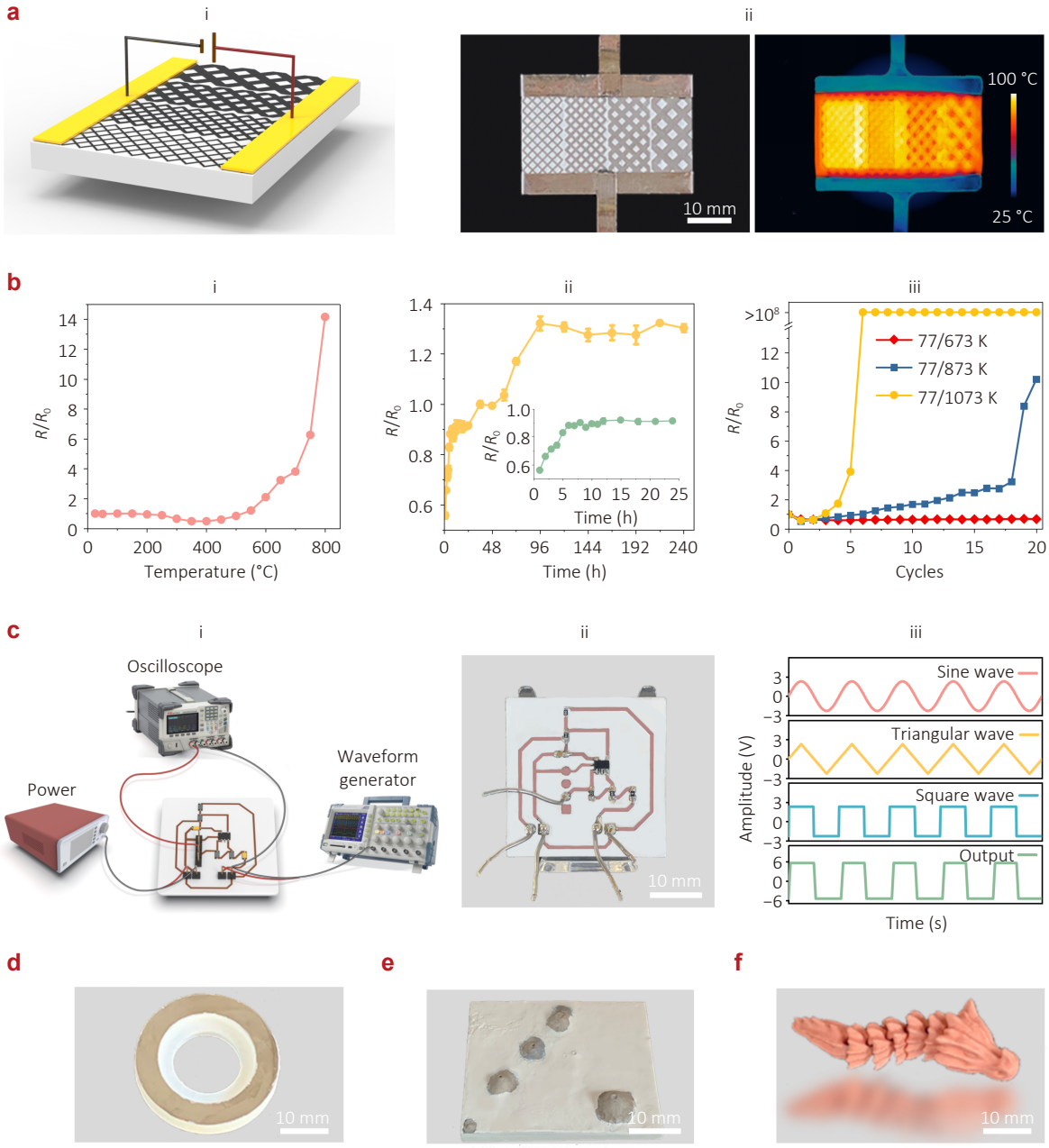

Fig. S4 | Demonstration of fabricated metallized ceramic structures. (a) Schematic structure of a Ni-P alloy-grid heater (a-i). Digital image of the heater composed of Ni-P alloy-grid conductor on Al_2O_3 ceramic and its IR images at a voltage (1.5 V) applied state (a-ii). The widths of the grid lines in four areas are 0.25 mm, 0.5 mm, 1 mm and 1.5 mm respectively. (b) Relative resistance variation (R/R_0) of metallized Ni-P alloy ceramic with the increase of temperature (b-i), as well as holding time at 400 °C (b-ii). The inset shows a magnified view in the range of 0-25 h. Measured R/R_0 after different cycles of thermal shocks (b-iii). The error bars denote the standard deviation (± s.d.) of the averaged values, n = 3 independent samples. (c) Schematic structure of a designed comparison circuit (c-i). Digital image of the copper-plated circuit board soldered with corresponding components of capacitors, resistors and operational amplifier (c-ii). The line width is 0.5 mm except one line connecting the operational amplifier (0.3 mm). Demonstration of results of the functional circuit (c-iii). Metallized ceramic structures of power battery connector (d), mountains in Mars (e) and dragon (f).

ceramic-based copper wire circuit board in this work has the advantages of dispensing with sputtering process (versus DPC), simple process control (versus DBC) and comparable bonding strength (versus AMB). Especially, there is no need to etch the circuit here. Hence, it is a good addition to the manufacturing methods of ceramic circuit board.

4 Methods

4.1 Materials

Alumina printing slurry containing micron and purity level of 99% alumina particles was purchased from Adventure technology, China. NiO nanoparticles (ϕ~100 nm, NiO, ≥

99.5% purity), Polyvinyl pyrrolidone (PVP, K30), α-terpilenol ($C_{10}H_{18}O$, ≥98% purity) were purchased from Aladdin, China. Copper electroless plating solution (mainly contains $CuSO_4$, ethylene diamine tetraacetate acid and formaldehyde) were purchased from Gaofan Electronic Technology Co., Ltd., China. Nickel electroless plating solution were purchased from Fakeda Surface Treatment Co., Ltd., China, which is mainly composed of $NiSO_4$, $NiCl_2$, malic acid, lactic acid, NaH_2PO_2 and amino acids, etc. High intensity Acrylate AB adhesive was purchased from Tegu New Material Co., Ltd., China. High-temperature resistant graphite conductive adhesive was purchased from Diantuo Polymer Materials Co., Ltd., China.

4.2 Metallized ceramic structures forming

For stereolithography, the slurry was processed in a commercial stereolithography printer of type ADT Ceram-D-F144 (Adventure technology, China, λ = 405 nm) under proper parameters (I_{UV} = 24 mW/cm^2, t_{curing} = 2.5 s, layer thickness τ = 50 μm). Thermal debinding was performed in a box furnace (KSL-1100X, HFKejing, China). The printed parts were heated to 600 °C gradually at the rate of 0.1–3 °C/min and held for 1–2 h at around 250 °C, 300 °C, 600 °C. Debond structures of grid heater, circuit board and power battery connector were implanted NiO nanoparticles on surface by means of screen-printing method, while simple dipping was performed on mountains in Mars and dragon. Co-sintering was performed in a high-temperature controlled atmosphere box furnaces of type GF17Q-11 (TianJin Muffle Technology Co., Ltd., China). The processed parts were densified at 1550 °C or 1600 °C for 2 h in pressureless atmosphere and the heating rate is 2–5 °C/min. After co-sintering, the radial and axial shrinkages are about 11% and 17% respectively. In addition, the density of co-sintered samples is nearly 95% of the theoretical density. Hydrogen reduction was performed in a pusher reduction furnace. The reduction gas is composed of 5 wt% H_2 and 95 wt% N_2, and the hybrid gas flow rate is 30 m^3/h. Parts were held in this reductive atmosphere for 1 h at 1000 °C.

For EP, the pH of the Ni-P bath is 4–5 and the temperature is heated to 90 °C during plating. The thickness of Ni-P alloy is nearly 2 μm after plating for 2 h. As for Cu film, the plating temperature is 40 °C and the thickness is about 3 μm when plating for 3 h.

4.3 Preparation of NiO nanoparticles dispersion solution

To prepare NiO nanoparticles ethanol dispersion solution for dipping process, the widely used polymer of PVP was added. That PVP was adsorbed on the particle surfaces would prevent particles from sedimentation and clustering again according to the steric stabilization effect. The ratio of NiO nanoparticles, PVP and ethanol is 100 mg : 600 mg : 10 mL in the dispersion solution. Taking 10 g/L concentration of NiO nanoparticles dispersion solution as an example, 600 mg PVP and 10 mL ethanol were mixed firstly before the dispersion process and then 100 mg NiO nanoparticles were added to the mixture. For further improving the quality of dispersion, the slurry was treated using an ultrasonic bath for 3 min. Experiment showed the solution had good stability that the apparent sedimentation did not happen in 10 min. NiO nanoparticles α-terpilenol dispersion solution with higher concentration was made to meet the requirement for screen printing. The ratio of NiO nanoparticles and α-terpilenol is 1000 mg : 10 mL in the dispersion solution.

4.4 Characterization

The X-ray diffraction measurements for the structure determination were carried out with Bruker DE/D8 Advance and Rigaku SmartLab SE and D/MAX-2600 using Cu Kα radiation. The sample was thinned using the FEI Scios 2 HiVac that integrates a field emission SEM with a focused ion beam (FIB). The STEM and HRTEM images to investigate the interfacial property were recorded by the FEI FEI Tecnai F20 instrument. The elementary composition (EDS mapping and line scanning) was analyzed by an energy-dispersive spectrometer (INCA Energy Coater, Oxford Instruments) coupled to the TEM. The scanning electron microscopy (ZEISS Gemini SEM 300, ZEISS, Germany; FEI-Apreo 2S HiVac, Thermo Fisher Scientific, USA) with energy-dispersive spectroscopy (Oxford Instruments) was used to investigate the morphologies, confirm distributions of Ni particles on surface as well as the situation of elements. The surface three-dimensional profile of metallized alumina samples were characterized using an Super Depth of Field Microscope (SDM, MOTIC Easyzoom, MOTIC, China). The bending strength of sintered Al_2O_3 substrates was obtained by three point bending tests (Testing standard: ASTM C1161-18 (2023)).

References

1. Zhang GM, Yu ZH, Song DS et al. Directly printed standing ceramic circuit boards for rapid prototyping of miniaturization and high-power of electronics. *Nat Commun* **16**, 5258 (2025).
2. Alhendi M, Alshatnawi F, Abbara EM et al. Printed electronics for extreme high temperature environments. *Addit Manuf* **54**, 102709 (2022).
3. Sahasrabudhe A, Dixit H, Majee R et al. Value added transformation of ubiquitous substrates into highly efficient and flexible electrodes for water splitting. *Nat Commun* **9**, 2014 (2018).
4. Zhang YB, Zhang T, Shi HB et al. Fabrication of flexible copper patterns by electroless plating with copper nanoparticles as seeds. *Appl Surf Sci* **547**, 149220 (2021).
5. Choi K, Kim SW, Lee JH et al. Eco-friendly glass wet etching for MEMS application: a review. *J Am Ceram Soc* **107**, 6497–6515 (2024).
6. Bai S, Serien D, Hu AM et al. 3D microfluidic surface-enhanced raman spectroscopy (SERS) chips fabricated by all-femtosecond-

laser-processing for real-time sensing of toxic substances. *Adv Funct Mater* **28**, 1706262 (2018).
7. Chu JN, Liu X, Zhang X et al. Annealing temperature dependence of mechanical and structural properties of chromium-gold films on the silica glass substrate. *Thin Solid Films* **774**, 139849 (2023).
8. Lv M, Liu JG, Wang SH et al. Higher-resolution selective metallization on alumina substrate by laser direct writing and electroless plating. *Appl Surf Sci* **366**, 227–232 (2016).
9. Lv HF, Dong X, Li RT et al. Super-dry reforming of methane using a tandem electro-thermocatalytic system. *Nat Chem* **17**, 695–702 (2025).
10. Weber ML, Jennings D, Fearn S et al. Thermal stability and coalescence dynamics of exsolved metal nanoparticles at charged perovskite surfaces. *Nat Commun* **15**, 9724 (2024).
11. Neagu D, Tsekouras G, Miller DN et al. *In situ* growth of nanoparticles through control of non-stoichiometry. *Nat Chem* **5**, 916–923 (2013).
12. Kothari M, Jeon Y, Miller DN et al. Platinum incorporation into titanate perovskites to deliver emergent active and stable platinum nanoparticles. *Nat Chem* **13**, 677–682 (2021).
13. Ye LT, Zhang MY, Huang P et al. Enhancing CO_2 electrolysis through synergistic control of non-stoichiometry and doping to tune cathode surface structures. *Nat Commun* **8**, 14785 (2017).
14. Rogers JL, Mangarella MC, D'Amico AD et al. Differences in the nature of active sites for methane dry reforming and methane steam reforming over nickel aluminate catalysts. *ACS Catal* **6**, 5873–5886 (2016).
15. Kumar A, Kanchan DR, Banerjee A et al. Synergistic effect of Ni exsolution and oxygen vacancies in $NiAl_2O_4$ for catalytic transfer hydrodeoxygenation of furfural to 2-methylfuran. *ACS Catal* **15**, 8239–8258 (2025).
16. Wang TR, Hu JY, Ouyang RH et al. Nature of metal-support interaction for metal catalysts on oxide supports. *Science* **386**, 915–920 (2024).
17. van Deelen TW, Hernández Mejía C, de Jong KP. Control of metal-support interactions in heterogeneous catalysts to enhance activity and selectivity. *Nat Catal* **2**, 955–970 (2019).
18. Monai M, Jenkinson K, Melcherts AEM et al. Restructuring of titanium oxide overlayers over nickel nanoparticles during catalysis. *Science* **380**, 644–651 (2023).
19. Hill BE, Misture ST. Atomic scale mechanisms of the reduction of nickel-magnesium aluminate spinels. *J Am Ceram Soc* **96**, 3603–3608 (2013).
20. Yu SY, Hu YW, Cui HJ et al. Ni-based catalysts supported on $MgAl_2O_4$ with different properties for combined steam and CO_2 reforming of methane. *Chem Eng Sci* **232**, 116379 (2021).
21. Üstünda E, Ret P, Subramanian R et al. In situ metal-ceramic microstructures by partial reduction reactions in the Ni-Al-O system and the role of ZrO_2. *Mater Sci Eng A* **195**, 39–50 (1995).
22. Neagu D, Oh TS, Miller DN et al. Nano-socketed nickel particles with enhanced coking resistance grown *in situ* by redox exsolution. *Nat Commun* **6**, 8120 (2015).
23. Kwon O, Sengodan S, Kim K et al. Exsolution trends and co-segregation aspects of self-grown catalyst nanoparticles in perovskites. *Nat Commun* **8**, 15967 (2017).
24. Hamada I, Uozumi A, Morikawa Y et al. A density functional theory study of self-regenerating catalysts $LaFe_{1-x}M_xO_{3-y}$ (M = Pd, Rh, Pt). *J Am Chem Soc* **133**, 18506–18509 (2011).
25. Yin P, Hu SL, Qian K et al. Quantification of critical particle distance for mitigating catalyst sintering. *Nat Commun* **12**, 4865 (2021).
26. Campbell CT, Mao ZT. Chemical potential of metal atoms in supported nanoparticles: dependence upon particle size and support. *ACS Catal* **7**, 8460–8466 (2017).
27. Liu LJ, Lu JY, Yang YH et al. Dealuminated Beta zeolite reverses Ostwald ripening for durable copper nanoparticle catalysts. *Science* **383**, 94–101 (2024).
28. Lou WC, Mao MM, Song KX et al. Low permittivity cordierite-based microwave dielectric ceramics for 5G/6G telecommunications. *J Eur Ceram Soc* **42**, 2820–2826 (2022).
29. Xu K, Sun Y, Chang Y et al. Regulation of bonding strength and activation mechanism of laser-induced metallization on Al_2O_3 ceramic surface. *Ceram Int* **51**, 56440–56454 (2025).

Acknowledgements

J.Z. acknowledges funding from the Distinguished Young Scholars of Natural Science Foundation of Heilongjiang under grant No. JQ2022F001. Y.C. was supported by the Young Elite Scientists Sponsorship Program by CAST under grant no. 2022QNRC001; the Youth Program of National Natural Science Foundation of China under grant No. 62105078; the Fundamental Research Funds of the Central University to the Harbin Engineering University under grant Nos. 3072024XX2702 and 3072025WD2503. S.L. acknowledges funding from the Youth Program of National Natural Science Foundation of China under grant No. 62405074.

Author contributions

J.Z. and Y.C. proposed the idea and initiated the project. Y.C. and K.Z designed the experimental process. K.Z, L.W., H.Z. and S.L. finished all the experiments and tests. K.Z., Y.C. and J.Z. analyzed the experimental data. K.Z. and Y.C. wrote the draft. J.Z. revised the draft.

Competing interests

The authors declare no competing interests.

Data availability

Any other data supporting the findings in this manuscript are available from the corresponding authors upon reasonable request.

Supplementary information

Supplementary information for this paper is available at
https://doi.org/10.29026/oep.2026.260008

Opto-Electronic Journals Group
www.oejournal.org

Scan for Article PDF